Conference Paper

Assessing a 35mm Fixed-Lens Sony Alpha-5100 Intrinsic Parameters Prior to, During, and Post UAV Flight Mission

Martinus E. Tjahjadi[1], Silvester S. Sai[1], and Fourry Handoko[2]

[1]Department of Geodesy, National Institute of technology (ITN Malang), Indonesia
[2]Departement of Industrial Engineering, National Institute of Technology (ITN) Malang, Indonesia

Abstract

A fixed focal length lens (FFL) camera with on-adjustable focal length is common companions for conducting aerial photography using unmanned aerial vehicles (UAVs) due to its superiority on optical quality and wider maximum aperture, lighter weight and smaller sizes. A wide-angle 35mm FFL Sony a5100 camera had been used extensively in our recent aerial photography campaign using UAV. Since this off-the-self digital camera is categorized into a non-metric one, a stability performance issue in terms of intrinsic parameters raises a considerably attention, particularly on variations of the lens principal distance and principal point's position relative to the camera's CCD/CMOS sensor caused by the engine and other vibrations during flight data acquisitions. A series of calibration bundle adjustment was conducted to determine variations in the principal distances and principal point coordinates before commencing, during, and after accomplishment of the flight missions. This paper demonstrates the computation of the parameters and presents the resulting parameters for three different epochs. It reveals that there are distinct discrepancies of the principal distances and principal point coordinates prior to, during, and after the mission, that peaked around 1.2mm for the principal distance, as well as around 0.4mm and 1.3mm along the x-axis and the y-axis of the principal point coordinates respectively. In contrast, the lens distortions parameters show practically no perturbations in terms of radial, decentering, and affinity distortion terms during the experiments.

Keywords: UAV, Non-metric, Camera, fixed-focal length Lens, Calibration

1. Introduction

A consumer grade entry-level Sony a5100 camera had been used extensively in our recent aerial photography campaign using UAV [1] for orthophoto mapping [2] and cadastral mapping [3], [4]. The Sony a5100 is a mirrorless compact that bundled with E PZ 16-50mm f/3.5-5.6 OSS zoom lens system (www.dpreview.com). Zoom lens consists of an assembly of various lens elements to allow for a range of focal lengths that enables a varying focal length to be produced from a single lens system which permits constant

focusing of the same relative aperture as focal length is changed [5]. For example, the focal length range of 16-50mm would spanned from the closest focal length of 16mm to the further focal length of 50mm. Despites all of benefits offered by zoom lens system, a presence of chromatic aberrations that could downgrade accuracies of lens distortion models [6]--[8] and off-the-self design of the zoom lens cannot be assumed to provide high mechanical stability [5]. This reason motivates us to replace the zoom lens system to a non-adjustable lens or fixed focal length lens (FFL). It is widely known that a fixed focal length lens is less likely to produce images with chromatic aberrations on which offers more superior optical quality [9]. Hence, a wide-angle 35mm FFL is attached to a body of Sony a5100 camera replacing its original zoom lens system.

Since the Sony a5100 off-the-self digital camera is categorized into a non-metric one, a stability performance issue in terms of intrinsic or interior orientation (IO) parameters raises a considerably attention, particularly on variations of the presumably fixed lens principal distance and principal point's position relative to the camera's CCD/CMOS sensor caused by the engine and other vibrations during flight data acquisitions. This paper investigates amount of deviation of FFL principal distances to the prescribed manufacturer release that is 35mm. utilization of the camera under conditions where vibrations, wind pressure and shock may be experienced during the campaign is subject to be investigated. Tied in with environmental extremity problems are demanded that the focal length lens undergoes immaterial deviations. Therefore, we quantify the deviations based on three different epochs: before the flight mission, during the missions and after the missions through conducting camera self-calibration on each epoch.

The Sony a5100 camera has not been specifically built for photogrammetry. There is no requirement for the manufacturer to align the lens element precisely, or to locate the lens in a pre-defined position relative to the CCD or CMOS sensor [10]. A metric quality issue of such a camera dominates mainly upon the degree of stability of the IO parameters [11], thus an accurate knowledge of the IO parameters is necessary [12], [13] for accurate photogrammetric products by using camera calibration. A camera calibration is a process of determining internal geometry parameters and optical characteristics of the camera which models the geometry of a complex camera system as an ideal pinhole camera [14]. There are numerous numbers of literatures on the digital camera calibration [6], [11], [15]. Among the existing camera calibration methods, an analytical self-calibration technique [16], [17] have been gained a popularity to calibrate the cameras in that it provides a means for detecting irregularities in camera calibration

when implemented in the camera operating environment for aerial photographing [18]--[20]. The self-calibration method is performed by means of the bundle adjustment [6] which provides a simultaneous determination of the interior and exterior orientation parameters, as well as the object point coordinates performed with or without a provision of known coordinates of control points [11], [13], [15], [21]--[23]. However, while object space control points of known 3D coordinates are available, calibration parameters can be recovered using space resection methods [24]--[26], relative orientation methods [27], [28], or bundle adjustment with fixed 3D coordinates.

Therefore, this paper investigates amount of deviations in the IO parameters particularly the calibrated focal length lens against the prescribed FFL manufacturer nominal value for the entry-level consumer grade Sony a5100 camera. Comparisons are conducted in three different environmental conditions: prior to and post mission flights, as well as during the flight mission. The ``prior to'' and ``post'' mission comparison aims to know deviations of the focal length lens when no external influences occurred. The ``during'' flight mission comparison aims to seek deviations due to engine vibrations and other vibrations between consecutive flight missions. Then, some characteristics of the FFL would be ascertained together with the principal point offset and lens distortion model. The self-calibration method and redundant flight paths will be employed [29]. Before elaborating the result, a brief discussion about the self-calibration method is following.

2. Method

2.1. Theoretical Foundation

The self-calibration procedure described in this paper is presented in the framework of analytical photogrammetric restitution which involves the perspective transformation between image and object space. It permits the IO parameters are recovered analytically, without the necessity for measured controlled points in object space [16], [17]. Considering the idealized camera configuration a collinearity equations provide the basis for such scheme [15]:

$$x' = x - x_0 - \Delta x = -c \frac{r_{11}(X - Xc) + r_{12}(Y - Yc) + r_{13}(Z - Zc)}{r_{31}(X - Xc) + r_{32}(Y - Yc) + r_{33}(Z - Zc)} = -c \frac{R1}{R3} \tag{1}$$

$$y' = y - y_0 - \Delta y = -c \frac{r_{21}(X - Xc) + r_{22}(Y - Yc) + r_{23}(Z - Zc)}{r_{31}(X - Xc) + r_{32}(Y - Yc) + r_{33}(Z - Zc)} = -c \frac{R2}{R3} \tag{2}$$

Equation (1) describes the perspective transformation between corrected or distortion free image points (x', y'), object space point (X, Y, Z), and perspective center (X_C, Y_C,

Z_C). The measured image coordinates (x, y) are subject to the departure corrections. The calibration terms consists of the IO parameters of the principal distance c and the principal point offset (x_0, y_0), and the image coordinate perturbation terms (Δx, Δy) which account for the departures from collinearity that arise from a number of sources. There are three main sources of physically interpretable departures from collinearity [15] such as symmetric radial distortion, decentring distortion, and affinity or in-plane image distortion. Error budgets of a displaced point on image will be a cumulative contribution of each perturbation [11]. Radial distortion is a radial displacement occurred on an imaged point from its theoretically correct position [12], [13]. This can be expressed by:

$$\Delta r = K_1 r^3 + K_2 r^5 + K_3 r^7 + \dots \tag{3}$$

$$r = \sqrt{(x - x_0)^2 + (y - y_0)^2} \tag{4}$$

Let r be the distance of the measured image point from the principal point (i.e. image radius), the radial distortion Δr is the radial displacement between the actual and the ideal locations of the image point, the Ks coefficients define the shape of the curve. The radial distortion is applied in terms of two components which relate each other [15]:

$$\frac{\Delta r}{r} = \frac{\Delta x_{rad}}{X'} = \frac{\Delta y_{rad}}{y'}, \Delta x_{rad} = X' \frac{\Delta r}{r}; \Delta y_{rad} = y' \frac{\Delta r}{r} \tag{5}$$

Decentring distortion is due to imperfect centering of the lens components and mis-alignment of individual lens element in compound lenses. The distortion is asymmetric with respect to the principal point and it can be compensated in the x-y directions by the following functions [15]:

$$\Delta x_{dec} = P_1 \left(r^2 + 2x'^2 \right) + 2P_2 x' y', \Delta y_{dec} = P_2 \left(r^2 + 2y'^2 \right) + 2P_1 x' y' \tag{6}$$

Δx_{dec} and Δy_{dec} are decentring distortion corrections, and P_1, P_2 are decentring parameters. Additional distortion, affinity and shear describe deviations in terms of orthogonality and uniform scale of the coordinate axes. An appropriate correction can be applied in x-y direction by the following function [15]:

$$\Delta x_{aff} = b_1 X' + b_2 y', \Delta y_{aff} = 0 \tag{7}$$

Two parameters of b1 and b2 account for differential scaling between the horizontal and vertical pixel spacing, and model non-orthogonality between the x-y axes. The individual terms of (4) -- (6) used to model a total perturbation on image coordinate [15]:

$$\Delta x = \Delta x_{rad} + \Delta x_{dec} + \Delta x_{aff}, \Delta y = \Delta y_{rad} + \Delta y_{dec} + \Delta y_{aff} \tag{8}$$

The correction model described in (1) is based on that the assumption the corrections are calculated by self-calibrating bundle adjustment. In the collinearity model (1), an association of points in the object space and image space are determined, then the perturbed distortions are added to the measured image coordinates.

2.2. Camera Lens Characteristics

This project uses entry-level consumer grade Sony a5100 camera equipped with an interchangeable lens system, a wide-angle 35mm FFL attached to the camera body. Specifications of the camera system are illustrated in Fig. 1 and Table 1 as follows.

| (a) | (b) | (c) |

Figure 1: A mirrorless Sony a5100 compact camera (*www.dpreview.com*): (a). bundled with E PZ 16-50mm f/3.5-5.6 OSS zoom lens system, (b). Camera body with its E-mount lens system, (c). Interchangeable FFL Sony FE 35mm F2.8 ZA Carl Zeiss T Lens.

TABLE 1: Main specification of the mirrorless Sony a5100 compact camera and the replaceable FFL lens.

Sony alpha a5100		Sony FE 35mm F2.8 ZA Carl Zeiss T Lens	
Main Specifications		**Main Specifications**	
Max resolution	6000 x 4000	Lens type	Prime lens
Image ratio w:h	3:2, 16:9	Focal length	35 mm
Effective pixels	24 megapixels	Lens mount	Sony FE
Sensor size APS-C	(23.5 x 15.6 mm)	Aperture	F2.8 - F22
Sensor type	CMOS	Minimum focus	0.35 m (13.78″)
Digital zoom	Yes (2X (Clear Image Zoom), 4X (digital zoom))	Maximum magnification	0.12×
Manual focus	Yes	Weight)	120 g (0.26 lb
Focal length multiplier	1.5×	Diameter	62 mm (2.44″)
Max shutter speed	1/4000 sec	Length	37 mm (1.46″)
Weight (inc. batteries)	283 g (0.62 lb / 9.98 oz)		

2.3. Field Measurement and Aerial Photography

This research is a part of the aerial mapping project using UAV to map Lowokwaru district in Malang City with its area spanned around 5000Ha. For camera self-calibration purposes, two calibration test fields are provided to assess the lens characteristics. The first calibration test field contains an array around 60 control points (Fig.2a) laid out regularly on the flat façade of a building which has small depth differences of approximately 20cm. This test field is used to calibrate the camera just before conducting the flight mission and just after the mission is done. But the second one has about 50 control points over 50m elevation differences located in the project area on the more rugged, undulated terrain. The second calibration test field constitutes approximately 20 per cent of average flying height above terrain which is the best choice for conducting camera self-calibration [29] (Fig.2b). These control points coordinates are measured using GPS-RTK to an accuracy of about 1cm (Fig.2b, Fig.2c, Fig.3a and Fig.3b). A purpose of giving control points 3D coordinates is to provide a more controllable calibration test area as a benchmark. The control points (Fig.2) are made up from a retro target that of a white concentric ring surrounded with dark background [30] to facilitate a possible highest accuracy of image coordinate measurements of control points on images.
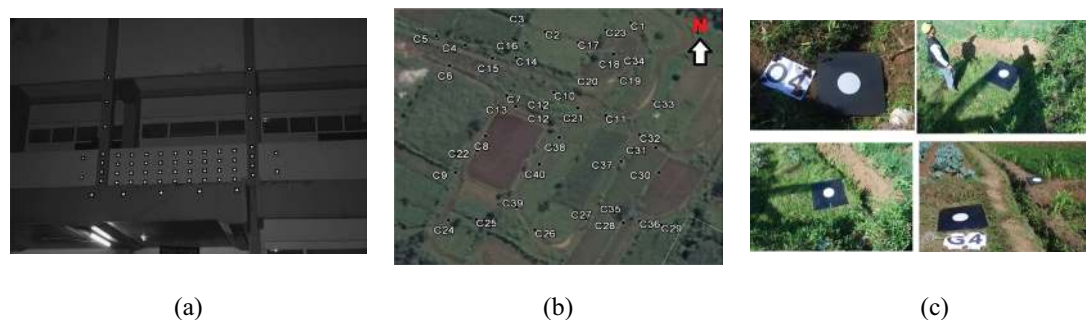

(a) (b) (c)

Figure 2: (a). Calibration test field on the building façade, (b). Calibration test field on the slanted and rugged topography, (c). Retro targets used as control points.

In the flight missions for photographing purposes, the camera is mounted to a fixed wing UAV, and one flight mission covers an area of about 300Ha for a flying height above the ground of 250m. Topographic variations of the area are spanning from flat ground to moderately undulated terrain. In every flight mission, the camera is positioned with nadir view looking. Flight plans are setup to have an approximately 85% forward overlap and around 60% side lap. When the flight mission covers the calibration area (Fig.2b), the mission is repeated once again for crossing previous flight courses. But this time the camera is positioned to a have a tilt of around 30 degrees off the nadir view. A strategy

(a)   (b)

Figure 3: GPS-RTK measurements on control points: (a). GPS base station, (b). GPS rover observing control points.

of having redundant cross flight plan and using the tilted camera accommodates the self-calibration requirement that the exposure networks should be convergent.

3. Results and Discussion

Now a stability of the FFL lens, the principal points offset, and lens distortion parameters will be ascertained using three image data sets: images taken prior to, during and post UAV flight mission. Before starting the first flight mission the camera self-calibration was conducted by photographing retro targets on the building façade (Fig.2a). During the flight missions, combinations of vertical and oblique images are collected for the camera self-calibration when the flight flied across the calibration test located in the project area (Fig.2b). Finally, after finishing the last flight mission, the camera self-calibration was performed again by photographing the retro target array on the building façade. These image data sets are processed using a free trial version of proprietary photogrammetric software. Results of the IO and lens distortion parameters are illustrated in Table 2 to Table 3, as well as in Fig.4 to Fig.6.

TABLE 2: Calibrated focal length and principal points.

IO Parameters	Before Flight Mission		During Flight Mission		After Flight Mission	
	Value	Standard Error	Value	Standard Error	Value	Standard Error
c (mm)	34.7495	2.26E-01	35.661	6.46E-01	35.3454	2.95E-01
x_0(mm)	-0.1233	1.24E-01	0.2684	3.51E-01	0.1404	1.90E-01
y_0(mm)	-0.3756	1.26E-01	-1.5595	3.44E-01	-0.2653	2.04E-01

Table 2 depicts the self-calibration results of the IO parameters in three different epochs. To quantify amount of deviations between the prescribed manufacturer release (e.g. 35mm) and the calibration results of the presumably fixed focal length lens at each
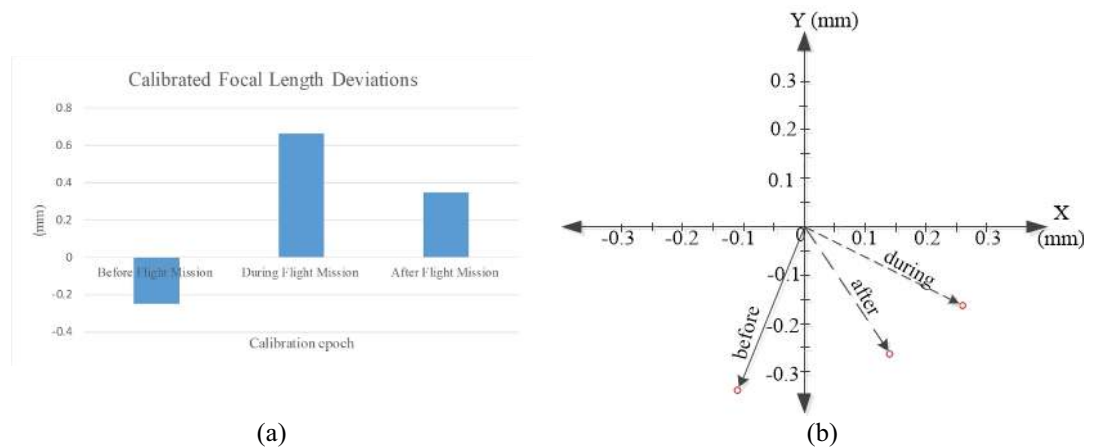
(a)   (b)

Figure 4: The IO parameters fluctuations prior to, during, and after the flight mission: (a). fixed focal length lens instabilities, (b). principal points instabilities.

epoch are compared. The focal length discrepancies of about 0.25mm, 0.66mm, and 0.34mm (Fig.4a) on each epoch show that instabilities of the FFL Lens still occurred. This indicates the lens is not resistant against the rapidly changing environmental conditions. Furthermore, the instabilities are also happened to the principal points offset (Table 2 and Fig.4b). If varying discrepancies are contrasted between two epochs (Fig.4b), it is shown that large deviations occurred when the camera is influenced by vibration of the platform (i.e. see epoch of ``during vs before'' and ``after vs during'') to peak at around 1.2mm. In contrast, a small amount of deviations of about 0.2mm (i.e. see epoch of ``after vs before'') is occurred when the camera is not on the mission. Therefore, this fact proofs that the IO parameters are not stable for the FFL Lens.

For the lens distortion parameters, on the other hand, immaterial differences are experienced in the three epochs (Table 3 and Fig.5). The radial distortion and decentring distortion parameters are relatively stable, but the affinity and shear distortion parameters experience very slight fluctuations. Again, deviations on the radial and decentring distortion parameters between two epochs are insignificant (Fig.6), but the affinity and shear parameters show a rather erratic in fluctuations and deviations. This finding shows that the lens distortion parameters of the FFL Lens is more resistant against vibrations and other external environmental conditions.

4. Conclusion

In summary, the manufacturer release of the fixed focal length Sony FE 35mm F2.8 ZA Carl Zeiss T Lens must be carefully anticipated when incorporated it in the photogrammetric UAV project mission. The lens' focal length and principal points are not

TABLE 3: Calibrated lens distortion model prior to, during, and after the flight mission.

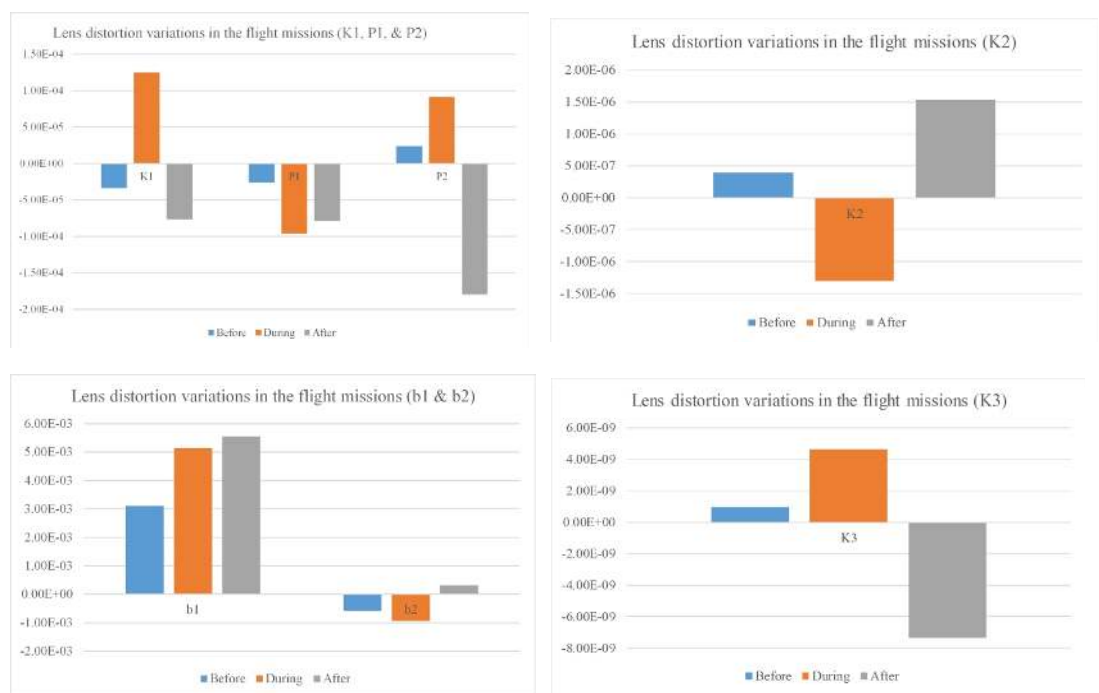| Lens Distortion Parameters	Before Flight Mission		During Flight Mission		After Flight Mission	
	Value	Standard Error	Value	Standard Error	Value	Standard Error
K_1	-3.37E-05	4.61E-05	1.25E-04	2.33E-05	-7.68E-05	7.94E-05
K_2	3.91E-07	9.98E-07	-1.30E-06	2.77E-07	1.53E-06	1.83E-06
K_3	9.97E-10	7.32E-09	4.65E-09	1.03E-09	-7.37E-09	1.40E-08
P_1	-2.61E-05	4.06E-05	-9.61E-05	4.59E-05	-7.82E-05	6.26E-05
P_2	2.40E-05	4.26E-05	9.16E-05	7.86E-05	-1.80E-04	8.60E-05
b_1	3.11E-03	2.68E-04	5.15E-03	1.13E-03	5.56E-03	7.00E-04
b_2	-5.88E-04	2.46E-04	-9.38E-04	1.40E-03	3.23E-04	5.51E-04

Figure 5: Fluctuations in lens distortion parameters before, during, and after the flight missions.

resistance against vibrations, carrying and handling, and unpredicted environment. But the lens distortion parameters show relatively stable values during the missions. The self-calibration method seems the most suitable way to calibrate of such cameras where photogrammetric accuracy requirements are demanded. This paper demonstrates the computation of the parameters and presents the resulting parameters for three different epochs. From a series of field test, it reveals that there are distinct discrepancies of the principal distances and principal point coordinates prior to, during, and after the mission that peaked around 1.2mm for the principal distance, as well as around 0.4mm and 1.3mm along the x-axis and the y-axis of the principal point coordinates respectively.
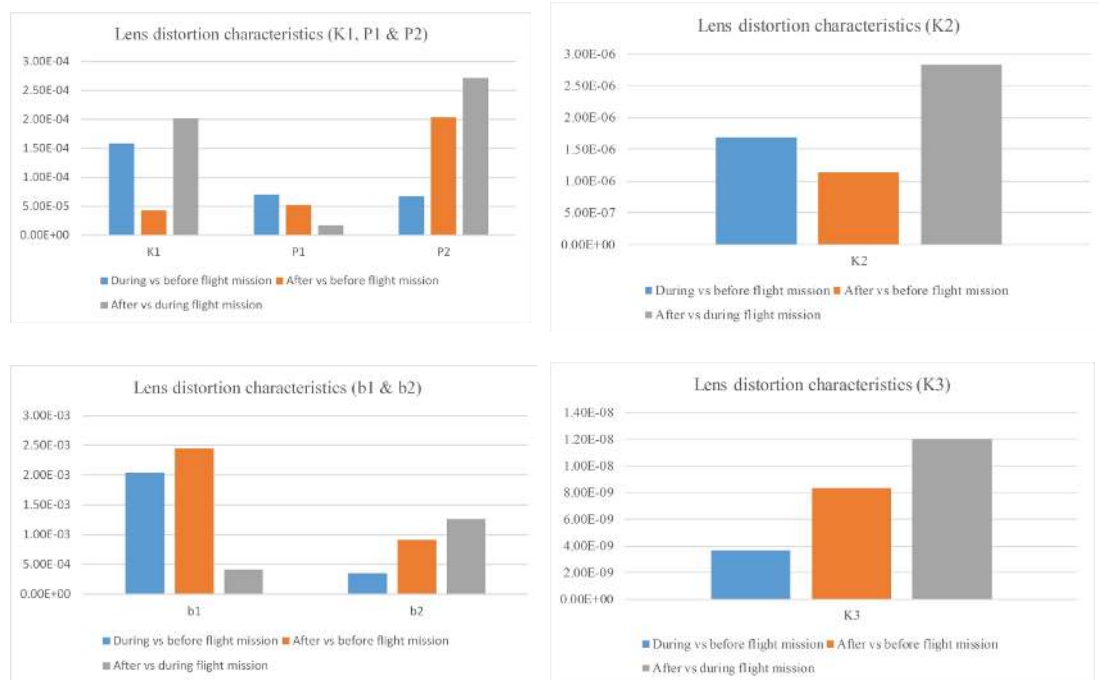
Figure 6: Lens distortion variations of the Lens before, during, and after the flight missions respectively: Deviations in lens distortion parameters between two epochs.

Acknowledgement

References

[1] M. E. Tjahjadi, F. Handoko, and S. S. Sai.(2017).Novel image mosaicking of UAV's imagery using collinearity condition. Int. J. Electr. Comput. Eng. **7**.

[2] S. S. Sai, M. E. Tjahjadi, and C. A. Rokhmana, ``Geometric accuracy assessments of orthophoto production from UAV aerial images,'' in *The 1st International Conference on Geodesy, Geomatics, and Land Administration 2019*, AIP Conference Proceeding, (Accepted).

[3] C. A. Rokhmana, I. A. Gumeidhidta, and M. E. Tjahjadi, ``Potential use of uav-based mapping system to accelerate the production of parcel boundary map in Indonesia,'' in *The 1st International Conference on Geodesy, Geomatics, and Land Administration 2019*, AIP Conference Proceeding, (Accepted).

[4] C. A. Rokhmana, M. E. Tjahjadi, and F. D. Agustina, ``Cadastral surveys with non-metric camera using UAV: a feasibility study,'' in *The 1st International Conference on Geodesy, Geomatics, and Land Administration 2019*, AIP Conference Proceeding, (Accepted).

[5] T. Luhmann, S. Robson, S. Kyle, and I. Harley, *Close Range Photogrammetry: Principles, Techniques and Applications* (Whittles Publishing, Scotland, UK, 2006).

[6] F. Remondino and C. Fraser. (2006). Int. Arch. Photogramm. Remote Sens. Spat. Inf. Sci. 36.

[7] B. Altena and T. Goedemé.(2014).ISPRS Ann. Photogramm. Remote Sens. Spat. Inf. Sci. II-5.

[8] H. Yanagi and H. Chikatsu. (2015). Int. Arch. Photogramm. Remote Sens. Spat. Inf. Sci. **XL-4/W5**.

[9] R. D. Fiete, ``Elements of Photogrammetric Optics,'' in *Manual of Photogrammetry 6th Edition*, edited by J. C. McGlone (American Society for Photogrammetry and Remote Sensing, Bethesda, Maryland, 2013), pp. 359--450.

[10] T. A. Clarke, X. Wang, and J. G. Fryer. (1998). Photogramm. Rec. 16, 293--312.

[11] C. S,Fraser. (2013). Photogramm. Eng. Remote Sens. 79, 381--388.

[12] A. Sampath, D. Moe, and J. Christopherson. (2012).Int. Arch. Photogramm. Remote Sens. Spat. Inf. Sci. **1**, 261--266.

[13] D. Moe, A. Sampath, J. Christopherson, and M. Benson. (2010). Int. Arch. Photogramm. Remote Sens. **38**, 395--400.

[14] R. Li, C. Toth, M. Mostafa, and C. V. Tao, ``Photogrammetric Applications: Mobile Mapping,'' in *Manual of Photogrammetry 6th Edition*, edited by J. C. McGlone (American Society for Photogrammetry and Remote Sensing, Bethesda, Maryland, 2013), pp. 1060--1074.

[15] T. Luhmann, C. Fraser, and H.-G. Maas.(2016). ISPRS J. Photogramm. Remote Sens. 115, 37--46.

[16] J. F. Kenefick. (1972).Photogramm. Eng. Remote Sens. 38, 1117--1126.

[17] J. M. Anderson. (1975). Photogramm. Eng. Remote Sens. 41, 1337--1348.

[18] B. Mélykuti and E. J. Kruck, Int. Arch. Photogramm. Remote Sens. Spat. Inf. Sci. **XL--1**, 253--256 (2014).

[19] J. G. Fryer, Photogramm. Eng. Remote Sensing **55**, 1751--1754 (1989).

[20] E. Honkavaara, Int. Arch. Photogramm. Remote Sens. Spat. Inf. Sci. **35-B1**, 166--172 (2004).

[21] C. S. Fraser, ISPRS J. Photogramm. Remote Sens. **52**, 149--159 (1997).

[22] C. S. Fraser, ``Photogrammetric Camera Component Calibration: A review of Analytical Technique,'' in *Calibration and Orientation of Cameras in Computer Vision*, edited by A. W. Gruen and T. S. Huang (Berlin Heidelberg: Springer-Verlag, 2010), pp. 93--121.

[23] C. S. Fraser, Int. Arch. Photogramm. Remote Sens. Spat. Inf. Sci. **36**, 9 (2005).

[24] M. E. Tjahjadi and F. Handoko, ``Single frame resection of compact digital cameras for UAV imagery,'' in *Deep Learning High Speed Processing technologies and Its Application on Electrical, Electronics, Computer science and Informatics for Humanity*, 4th International Conference on Electrical Engineering, Computer Science and Informatics (EECSI), edited by M. A. Riyadi et al. (IEEE, Yogyakarta, 2017), pp. 409-413.

[25] M. E. Tjahjadi, ARPN J. Eng. Appl. Sci.**11**, 3449--3455 (2016).

[26] M. E. Tjahjadi and F. D. Agustina, ``Single image orientation of UAV's imagery using orthogonal projection model,'' in *Achieving Sustainability through Digital Earth*, 2017 International Symposium on Geoinformatic (ISyG), (IEEE, Malang, 2017), pp.19-24.

[27] M. E. Tjahjadi and F. D. Agustina, ``A Relative Rotation between Two Overlapping UAV's Images,'' in *Toward the Next Generation of technology*, 5th International Conference on Electrical Engineering, Computer Science and Informatics (EECSI), edited by A. Yudhana et al. (IEEE, Malang, 2018), pp. 658--663.

[28] M. E. Tjahjadi and F. D. Agustina, Int. J. Adv. Intell. Informatics **5**, 24--39 (2019).

[29] M. E. Tjahjadi, S. S. Sai, and C. A. Rokhmana, ``Assessing stability performance of non-metric camera's lens distortion model during uav flight missions,'' in *The 1st International Conference on Geodesy, Geomatics, and Land Administration 2019*, AIP Conference Proceeding, (Accepted).

[30] T. A. Clarke and X. Wang, ``Extracting high-precision information from CCD images,'' in *Proc. ImechE Conf., Optical methods and data processing for heat and fluid flow* (City University, 1998), pp. 311--320.